Surface-Enhanced Infrared Absorption Spectroscopy of Bacterial Nitric Oxide Reductase under Electrochemical Control Using Vibrational Probe of Carbon Monoxide

Masaru Kato,[*,†,‡,§] *Shogo Nakagawa,*[‡] *Takehiko Tosha,*[||] *Yoshitsugu Shiro,*[#] *Yuya Masuda,*[‡] *Kou Nakata,*[†,‡] *Ichizo Yagi**[*,†,‡,§]

[†] Faculty of Environmental Earth Science and [‡] Graduate School of Environmental Science, Hokkaido University, N10W5, Kita-ku, Sapporo 060-0810, Japan. [§] Global Research Center for Environment and Energy based on Nanomaterials Science (GREEN), National Institute for Materials Science (NIMS), Tsukuba 305-0044, Japan. [||] RIKEN SPring-8 Center, Kouto, Sayo, Hyogo 679-5148, Japan. [#]Graduate School of Life Science, University of Hyogo, Hyogo 678-1297, Japan.

AUTHOR INFORMATION

Corresponding Authors

*E-mail: masaru.kato@ees.hokudai.ac.jp (M.K.)

*E-mail: iyagi@ees.hokudai.ac.jp (I.Y.)

ABSTRACT. Nitric oxide reductases (NORs) reduce nitric oxide to nitrous oxide in the denitrification pathway of the global nitrogen cycle. NORs contain four iron cofactors and the NO reduction occurs at the heme b_3/non-heme Fe_B binuclear active site. The determination of reduction potentials of the iron cofactors will help us elucidate the enzymatic reaction mechanism. However, previous reports on these potentials remain controversial. Herein, we performed electrochemical and surface-enhanced infrared absorption (SEIRA) spectroscopic measurements of *Pseudomonas aeruginosa* NOR immobilized on gold electrodes. Cyclic voltammograms exhibited two reduction peaks at –0.11 and –0.44 V vs. SHE, and a SEIRA spectrum using a vibrational probe of CO showed a characteristic band at 1972 cm^{-1} at –0.4 V vs. SHE, which was assigned to νCO of heme b_3–CO. Our results suggest that the reduction of heme b_3 initiates the enzymatic NO reduction.

TOC GRAPHICS

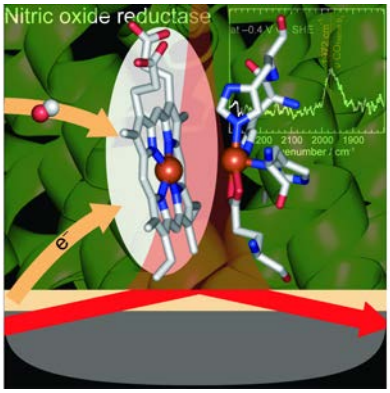

Denitrification is an energy generation process for certain bacteria under low-oxygen conditions from nitrate instead of molecular oxygen and an important process for the global nitrogen cycle. In the denitrification process, the sequential reduction of nitrate to dinitrogen ($NO_3^- \rightarrow NO_2^- \rightarrow NO \rightarrow N_2O \rightarrow N_2$) is carried out by several different metalloenzymes including nitric oxide reductase (NOR).[1] NORs are transmembrane proteins (**Figure 1a**) and convert highly cytotoxic nitric oxide to nitrous oxide ($2NO + 2H^+ + 2e^- \rightarrow N_2O + H_2O$).[2–4] For pathogenic bacteria such as *Pseudomonas aeruginosa*, the highly efficient NO reduction is crucial to surviving inside hosts.[5] Understanding the efficient reaction mechanism will provide insights into how NO dynamics are controlled in biological processes. The elucidation of the enzymatic reaction mechanism can also offer important guidance for developing highly efficient and selective electrocatalysts for the electrochemical nitrate reduction to N_2, which is a promising industrial approach to remove nitrate ions from nitrate-contaminated groundwater and wastewater.[6,7] NO is an important intermediate for electrochemical nitrate reduction and the selective NO reduction to N_2O using electrocatalysts can lead to the desired final product of harmless N_2 but not NH_3 or NH_2OH.[8–11]

The enzymatic NO reduction is known to occur at the binuclear iron reaction center containing a high-spin heme (heme b_3) and a non-heme iron (Fe_B) (**Figure 1b**). This reaction center receives electrons from the electron transfer iron cofactors of heme *b* and heme *c*, which is placed in a small subunit NorC (**Figure 1a**) and accepts electrons from physiological electron mediators such as cytochrome c_{551}.[2,4] The NOR reaction mechanism remains under debate and three mechanisms for the NO reduction have been proposed (**Figure 1c**): *cis*-heme b_3 mechanism, the second NO molecule attacks the nitrogen atom of the NO molecule coordinated to heme b_3 iron; *trans* mechanism, one NO molecule is bound to each iron and then the two coordinated NO molecules are coupled to form the N–N bond; *cis*-Fe_B mechanism, two NO molecules are

coordinated to the Fe_B iron, followed by reductive N-N coupling. To understand the reaction mechanism, electrochemical properties of the four iron cofactors of NORs have been studied using spectroelectrochemical titration[12–15] and protein film electrochemistry (PFE),[16,17] which provides current–potential responses of redox-active metalloenzymes immobilized on the electrode surface.[18–20] These techniques revealed that the four iron cofactors are sequentially reduced and the four-electron-reduced NOR is the active form for the NO reduction.[14,17] However, the assignments of previously reported redox potentials were unclear owing to the lack of monitoring specific molecular signatures during the redox measurements. Since vibrational spectroscopy is useful for the characterization of the active site structure, vibrational spectroscopic measurements coupled with the PFE would be ideal to understand accurate redox behavior of metalloenzymes at the electrode interface.[21–28]

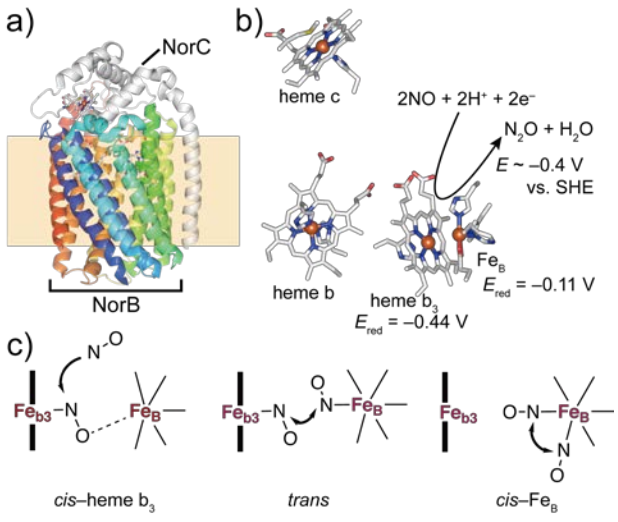

Figure 1. (a) Overall structure of cNOR from *P. aeruginosa* (PDB: 3O0R)[4] and (b) the arrangement of four iron cofactors in cNOR: heme *c*, heme *b*, heme b_3 and Fe_B. The reduction potentials for heme b_3 and Fe_B and the onset potential for the enzymatic NO reduction are shown.

These potential were determined in this work. (c) Three proposed reaction mechanisms for the enzymatic NO reduction: *cis*–heme b_3, *trans* and *cis*–Fe_B.

Herein, we report the PFE of a cytochrome c-dependent NOR (cNOR) under catalytic and non-catalytic conditions and SEIRA spectroscopy of cNOR under electrochemical control. The cNOR was isolated from *P. aeruginosa*[4,29] and immobilized on a SEIRA-active gold thin film[30,31] directly or *via* a linker (**Figure 2a**), where the gold film had a roughness factor ranging between 2.5 and 3.5 (**Figure S2**). For the direct immobilization of the cNOR (cNOR–Au), an aqueous solution containing the cNOR was drop-cast onto the bare Au film. For the immobilization via linkers (cNOR–NHCO–Au), the cNOR solution was drop-cast onto the Au film that was modified with a self-assembled monolayer (SAM) of 3-mercaptopropionic acid (HOOC–Au), and then incubated with covalent bonding reagents of *N*-hydroxysuccinimide (NHS) and 1-ethyl-3-(3-dimethylaminopropyl)carbodiimide hydroxide (EDC).[32] The formation of the SAM on the Au film was confirmed by SEIRA spectroscopy (**Figure S3**) and electrochemical reductive desorption, which gave a surface density of 3.29 nmol cm^{-2} for the linker (**Figure S4**).

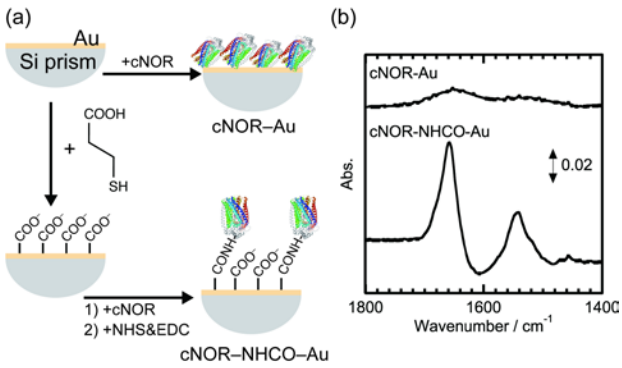

Figure 2. (a) Schematic representation of the preparation of *c*NOR–modified Au electrodes with/without the SAM of 3-mercaptopropionic acid. (b) SEIRA spectra of cNOR–Au and cNOR–

NHCO–Au in a 50 mM MES-buffered electrolyte solution containing 50 mM K_2SO_4 in H_2O at pH 6.5 under Ar. The corresponding electrodes without cNOR were used for reference spectra.

SEIRA spectroscopy of cNOR–Au and cNOR–NHCO–Au revealed that transmembrane helices of the cNOR were vertically oriented to the Au film with/without the SAM. SEIRA spectra of cNOR–Au and cNOR–NHCO–Au showed two characteristic peaks at ca. 1655 cm^{-1} for the amide I band and 1540 cm^{-1} for the amide II band (**Figure 2b**). Amide I bands at ~1650 cm^{-1} indicate that there are dehydrated helical amide groups.[33,34] Thus, it is most likely that the cNOR has its native structure with transmembrane α-helices (**Figure 1a**)[4] on the Au surface with/without the SAM. Notably, the SEIRA spectra of cNOR–Au and cNOR–NHCO–Au showed a stronger amide I band and a weaker amide II band: amide I/amide II band peak intensity ratios were determined to be 1.8 to 1.9 for the SEIRA spectra of cNOR–Au and cNOR–NHCO–Au. These ratios were higher than the ratio of ca. 1.6 determined for a FT-IR transmission spectrum of the cNOR in solution (**Figure S5**). In the α-helix, the amide I mode is known to be parallel to the helix axis but the amide II mode perpendicular.[35] Thus, the transmembrane helices were oriented perpendicular to the Au surface because of the surface selection rule.[36,37]

The band peaks of cNOR–NHCO–Au were higher than those of cNOR–Au. This difference originates from differences in protein structure and/or orientation on the Au surface. For the cNOR–Au electrode, the enzyme could be tethered to the Au surface *via* the surface-exposed cysteine, Cys86, on the cNOR (**Figure S6**),[4] making the transmembrane helices perpendicular to the Au surface. Such surface-exposed cysteine residues were reported to keep functioning without protein denaturation even on the metal surface.[38] In the case of cNOR–NHCO–Au, surface-

exposed amine groups such as lysine on the cNOR (**Figure S7**) could form covalent bonds with terminal carboxylate groups of the SAM on the Au surface. It is known that the protein orientation on SAMs can be controlled by electrostatic interactions with terminal functional groups of SAMs.[20,32,39] Thus, the cNOR was anchored to the HOOC-terminated SAM and its α-helices tended to be more vertically oriented to the Au surface than those for cNOR–Au, resulting in the higher peaks for cNOR–NHCO–Au. Note that no clear peaks on amide bond vibrational modes were observed for the cNOR that was covalently bonded to an H_2N-terminated SAM of 2-aminoethanethiol on the Au substrate (**Figure S8**). It seems that the orientation of the cNOR is highly sensitive to the terminal group of SAMs and α-helices of the cNOR may be perpendicular to the HOOC-terminated SAM but not to the H_2N-terminated SAM.

The redox behavior of iron cofactors of the cNOR was captured in cyclic voltammograms (CVs) in the absence of the substrate NO. CVs of cNOR–Au were recorded in a buffered aqueous solution at pH 7 under Ar and two reduction peaks were observed at –0.11 and –0.44 V vs. SHE (**Figure 3a**). The same redox behavior was reported for the cNOR from *P. nautica* immobilized on a pyrolytic graphite electrode under Ar,[17] suggesting that cNORs are redox-active not only on carbon but also on Au. The integration of the reduction peak at –0.44 V vs. SHE gave a protein surface density of 12.2 pmol cm^{-2}. Unfortunately, no clear reduction peak was observed for cNOR–NHCO–Au, suggesting that much fewer amounts of the protein were immobilized *via* the SAM than those for the cNOR-Au.

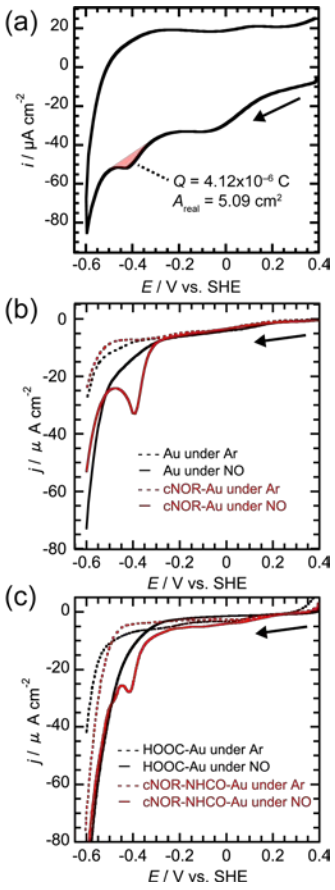

Figure 3. (a) A CV of cNOR–Au under Ar. (b) LSVs of the bare Au under Ar (the dotted line in black) and NO (the solid line in black) and cNOR–Au under Ar (the dotted line in red) and NO (the solid line in red). (c) LSVs of HOOC–Au without cNOR under Ar (the dotted line in black) and NO (the solid line in black) and cNOR–NHCO–Au under Ar (the dotted line in red) and NO (the solid line in red). CVs and LSVs were recorded at 0.5 V s^{-1} and 0.02 V s^{-1}, respectively, in a 50 mM MES-buffered electrolyte solution containing 50 mM K_2SO_4 at pH 6.5. The arrows indicate the sweeping direction.

To understand the electrocatalytic activity of the cNOR for the NO reduction, linear sweep voltammograms (LSVs) of cNOR-modified electrodes were recorded under NO. The cNOR-immobilized electrodes of cNOR–Au and cNOR–NHCO–Au showed catalytic cathodic currents with an onset potential of ca. –0.35 V vs. SHE under NO (**Figures 3b** and **3c**). Similar electrocatalytic behavior was reported on *P. nautica* cNOR immobilized on a pyrolytic graphite electrode.[17] No catalytic current was observed for the electrodes unmodified with cNOR under NO or those modified with the cNOR under Ar (**Figure 3b** and **3c**). Thus, the electrocatalytic currents originate from the enzyme on the electrode.

The electrocatalytic activity of the cNOR anchored to the SAM was higher than that on the electrode surface without the SAM. A turnover frequency of the cNOR was determined to be approximately 0.52 s^{-1} from chronoamperometry measurements of cNOR–Au at –0.4 V vs. SHE under NO (**Figure S9**). Notably, both of cNOR–Au and cNOR–NHCO–Au gave the same order of magnitude in catalytic current densities for the NO reduction (**Figures 3b** and **3c**), even though the cNOR–NHCO–Au electrode kept fewer protein amounts than the cNOR–Au electrode, as mentioned above. These results indicate that the catalytic activity of cNOR–NHCO–Au was higher than that of cNOR–Au and the protein orientation for cNOR–NHCO–Au was more suitable for interfacial electron transfer from the electrode to the enzyme. For cNOR–Au, the enzyme could be tethered to the Au surface *via* Cys86 (**Figure S6**), where the electron transfer cofactor heme *c*, which can accept electrons from cytochrome c_{551} under physiological conditions,[2] was placed away from the electrode surface. Thus, it is most likely that the hydrophilic domain of the subunit NorC that contains heme c^4 faced the Au surface for cNOR–NHCO–Au (**Figure 2a**).

To assign the two reduction peaks observed in the CV, potential-dependent SEIRA spectra of cNOR–NHCO–Au were recorded using carbon monoxide (CO), which serves as a vibrational

probe of heme protein active sites with Fe^{II}.[40] The electrochemical reduction of heme b_3 from Fe^{III} to Fe^{II} can be tracked by the νCO band in potential-dependent SEIRA spectra of the cNOR, leading us to determine the reduction potentials of the binuclear iron reaction center. During applying potential steps from 0 to –0.4 V vs. SHE, a characteristic peak appeared at 1972 cm^{-1} at –0.4 V vs. SHE (**Figure 4**). This peak was assigned to the stretching mode of the CO that bonds to heme b_3 (heme b_3–CO), not to that for Fe_B–CO (ca. 2066 cm^{-1}).[41,42] Thus, the reduction peak at –0.44 vs. SHE (**Figure 3a**) was associated with the reduction of the iron center from Fe^{III} to Fe^{II} for heme b_3 (**Figure 1b**). The other reduction peak observed at –0.11 V vs. SHE (**Figure 3a**) could be assigned to the reduction of Fe^{III} to Fe^{II} for Fe_B because electron transfer heme *b* and heme *c* have much more positive redox potentials. [14,17]

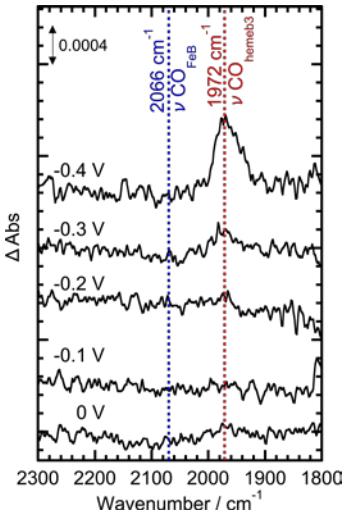

Figure 4. Potential-dependent SEIRA spectra of CO-adsorbed cNOR–NHCO–Au applying potentials from 0 to –0.4 V vs. SHE. A 50 mM MES-buffered electrolyte solution containing 50 mM K_2SO_4 in H_2O at pH 6.5 was used as the electrolyte solution. A SEIRA spectrum of HOOC–Au without cNOR at the corresponding potential was used as the reference spectrum.

The determination of the onset potential for the electrocatalytic NO reduction and the reduction potentials of heme b_3 and Fe_B enable us to exclude the *cis*-Fe_B mechanism. The onset potential at ca. –0.35 V vs. SHE was close to the reduction potential of the heme b_3 at –0.44 V vs. SHE, indicating that the electrocatalytic NO reduction is initiated by the reduction of heme b_3. Our results are in good agreement with the previous experimental results that indicate that the four-electron-reduced NOR is the active form for the NO reduction.[14,17] Thus, heme b_3 should be involved in the enzymatic NO reduction, which means that the *cis*-Fe_B mechanism is highly unlikely. Although it was mentioned that heme Fe^{II}–NO complexes are too stable to initiate the NO reduction,[14] recent studies on NOR models suggested that the N–O bond of the heme b_3 Fe^{II}–NO can be weakened by the interaction between the terminal nitrosyl O-atom and Fe_B, where Fe_B serves as an electron donor and a Lewis acid.[43–46] In such a scenario, the reduced heme b_3–NO species can be involved in the NO reduction by NORs.

In summary, the PFE of the cNOR from *P. aeruginosa* and the SEIRA spectroscopy of the CO-adsorbed cNOR revealed that the reduction of Fe^{III} to Fe^{II} for heme b_3 was observed at –0.44 V vs. SHE and this reduction potential was close to the onset potential for the electrocatalytic NO reduction. These findings suggest that heme b_3 should be involved in the enzymatic NO reduction and the *cis*-Fe_B mechanism is highly unlikely. Further experimental studies on SEIRA spectroscopy of cNOR-modified electrodes under catalytic conditions are underway in our group to gain more mechanistic insights into the enzymatic NO reduction.

ASSOCIATED CONTENT

Supporting Information.

The following files are available free of charge on the ACS Publications website at DOI: xxx.

Experimental methods, cyclic voltammograms, SEIRA spectra and a chronoamperogram (PDF)

AUTHOR INFORMATION

Corresponding Authors

*E-mail: masaru.kato@ees.hokudai.ac.jp (M.K.)

*E-mail: iyagi@ees.hokudai.ac.jp (I.Y.)

Notes

The authors declare no competing financial interests.

ORCID

Masaru Kato: 0000-0002-2845-3525

Ichizo Yagi: 0000-0002-4005-9440

ACKNOWLEDGMENTS

The authors thank Shingo Mukai, Katsuhisa Ishikawa, Takahiko Hasegawa, and Yusuke Kawamura (Technical Division, Institute for Catalysis, Hokkaido University) for their technical supports on SEIRA spectroscopy and electrochemistry setups. The authors also thank Dr. Minoru Kubo (RIKEN SPring-8 Center) for fruitful discussion and suggestions. This work was supported by Grant-in-Aid for Young Scientists (B) (No. 16K20882 to M.K.) and a MEXT Program for Development of Environmental Technology using Nanotechnology from the Ministry of Education, Culture, Sports, Science and Technology, Japan.

REFERENCES

(1) Canfield, D. E.; Glazer, A. N.; Falkowski, P. G. The Evolution and Future of Earth's Nitrogen Cycle. *Science* **2010**, *330*, 192–196.

(2) Hino, T.; Nagano, S.; Sugimoto, H.; Tosha, T.; Shiro, Y. Molecular Structure and Function of Bacterial Nitric Oxide Reductase. *BBA Bioenergetics* **2012**, *1817*, 680–687.

(3) Tosha, T.; Shiro, Y. Crystal Structures of Nitric Oxide Reductases Provide Key Insights into Functional Conversion of Respiratory Enzymes. *IUBMB Life* **2013**, *65*, 217–226.

(4) Hino, T.; Matsumoto, Y.; Nagano, S.; Sugimoto, H.; Fukumori, Y.; Murata, T.; Iwata, S.; Shiro, Y. Structural Basis of Biological N_2O Generation by Bacterial Nitric Oxide Reductase. *Science* **2010**, *330*, 1666–1670.

(5) Kakishima, K.; Shiratsuchi, A.; Taoka, A.; Nakanishi, Y.; Fukumori, Y. Participation of Nitric Oxide Reductase in Survival of Pseudomonas Aeruginosa in LPS-Activated Macrophages. *Biochem. Biophys. Res. Commun.* **2007**, *355*, 587–591.

(6) Rosca, V.; Duca, M.; de Groot, M. T.; Koper, M. T. M. Nitrogen Cycle Electrocatalysis. *Chem. Rev.* **2009**, *109*, 2209–2244.

(7) Duca, M.; Koper, M. T. M. Powering Denitrification: The Perspectives of Electrocatalytic Nitrate Reduction. *Energy Environ. Sci.* **2012**, *5*, 9726–9742.

(8) Kato, M.; Okui, M.; Taguchi, S.; Yagi, I. Electrocatalytic Nitrate Reduction on Well-Defined Surfaces of Tin-Modified Platinum, Palladium and Platinum-Palladium Single

Crystalline Electrodes in Acidic and Neutral Media. *J. Electroanal. Chem.* **2017**, *800*, 46–53.

(9) Chen, Y.; Zhu, H.; Rasmussen, M.; Scherson, D. Rational Design of Electrocatalytic Interfaces: The Multielectron Reduction of Nitrate in Aqueous Electrolytes. *J. Phys. Chem. Lett.* **2010**, *1*, 1907–1911.

(10) Yoshioka, T.; Iwase, K.; Nakanishi, S.; Hashimoto, K.; Kamiya, K. Electrocatalytic Reduction of Nitrate to Nitrous Oxide by a Copper-Modified Covalent Triazine Framework. *J. Phys. Chem. C* **2016**, *120*, 15729–15734.

(11) Yang, J.; Calle-Vallejo, F.; Duca, M.; Koper, M. T. M. Electrocatalytic Reduction of Nitrate on a Pt Electrode Modified by P-Block Metal Adatoms in Acid Solution. *ChemCatChem* **2013**, *5*, 1773–1783.

(12) Grönberg, K. L. C.; Roldán, M. D.; Prior, L.; Butland, G.; Cheesman, M. R.; Richardson, D. J.; Spiro, S.; Thomson, A. J.; Watmough, N. J. A Low-Redox Potential Heme in the Dinuclear Center of Bacterial Nitric Oxide Reductase: Implications for the Evolution of Energy-Conserving Heme−Copper Oxidases. *Biochemistry* **1999**, *38*, 13780–13786.

(13) Field, S. J.; Prior, L.; Roldán, M. D.; Cheesman, M. R.; Thomson, A. J.; Spiro, S.; Butt, J. N.; Watmough, N. J.; Richardson, D. J. Spectral Properties of Bacterial Nitric-Oxide Reductase: Resolution of pH-dependent Forms of the Active Site Heme b_3. *J. Biol. Chem.* **2002**, *277*, 20146–20150.

(14) Timoteo, C. G.; Pereira, A. S.; Martins, C. E.; Naik, S. G.; Duarte, A. G.; Moura, J. J. G.; Tavares, P.; Huynh, B. H.; Moura, I. Low-Spin Heme b_3 in the Catalytic Center of Nitric Oxide Reductase from Pseudomonas Nautica. *Biochemistry* **2011**, *50*, 4251–4262.

(15) Field, S. J.; Roldan, M. D.; Marritt, S. J.; Butt, J. N.; Richardson, D. J.; Watmough, N. J. Electron Transfer to the Active Site of the Bacterial Nitric Oxide Reductase Is Controlled by Ligand Binding to Heme b_3. *BBA Bioenergetics* **2011**, *1807*, 451–457.

(16) Cordas, C. M.; Pereira, A. S.; Martins, C. E.; Timóteo, C. G.; Moura, I.; Moura, J. J. G.; Tavares, P. Nitric Oxide Reductase: Direct Electrochemistry and Electrocatalytic Activity. *ChemBioChem* **2006**, *7*, 1878–1881.

(17) Cordas, C. M.; Duarte, A. G.; Moura, J. J. G.; Moura, I. Electrochemical Behaviour of Bacterial Nitric Oxide Reductase-Evidence of Low Redox Potential Non-Heme Fe_B Gives New Perspectives on the Catalytic Mechanism. *BBA Bioenergetics* **2013**, *1827*, 233–238.

(18) Kato, M.; Zhang, J. Z.; Paul, N.; Reisner, E. Protein Film Photoelectrochemistry of the Water Oxidation Enzyme Photosystem II. *Chem. Soc. Rev.* **2014**, *43*, 6485.

(19) Armstrong, F. A.; Belsey, N. A.; Cracknell, J. A.; Goldet, G.; Parkin, A.; Reisner, E.; Vincent, K. A.; Wait, A. F. Dynamic Electrochemical Investigations of Hydrogen Oxidation and Production by Enzymes and Implications for Future Technology. *Chem. Soc. Rev.* **2009**, *38*, 36–51.

(20) Saboe, P. O.; Conte, E.; Farell, M.; Bazan, G. C.; Kumar, M. Biomimetic and Bioinspired Approaches for Wiring Enzymes to Electrode Interfaces. *Energy Environ. Sci.* **2017**, *10*, 14–42.

(21) Khoa Ly, H.; Sezer, M.; Wisitruangsakul, N.; Feng, J.-J.; Kranich, A.; Millo, D.; Weidinger, I. M.; Zebger, I.; Murgida, D. H.; Hildebrandt, P. Surface-Enhanced Vibrational Spectroscopy for Probing Transient Interactions of Proteins with Biomimetic Interfaces: Electric Field Effects on Structure, Dynamics and Function of Cytochrome c. *FEBS J.* **2011**, *278*, 1382–1390.

(22) Gutiérrez-Sanz, O.; Marques, M.; Pereira, I. A. C.; De Lacey, A. L.; Lubitz, W.; Rüdiger, O. Orientation and Function of a Membrane-Bound Enzyme Monitored by Electrochemical Surface-Enhanced Infrared Absorption Spectroscopy. *J. Phys. Chem. Lett.* **2013**, *4*, 2794–2798.

(23) Kriegel, S.; Uchida, T.; Osawa, M.; Friedrich, T.; Hellwig, P. Biomimetic Environment to Study E. Coli Complex I through Surface-Enhanced IR Absorption Spectroscopy. *Biochemistry* **2014**, *53*, 6340–6347.

(24) Heidary, N.; Utesch, T.; Zerball, M.; Horch, M.; Millo, D.; Fritsch, J.; Lenz, O.; Von Klitzing, R.; Hildebrandt, P.; Fischer, A.; Mroginski, M. A.; Zebger, I. Orientation-Controlled Electrocatalytic Efficiency of an Adsorbed Oxygen-Tolerant Hydrogenase. *PLoS One* **2015**, *10*, 143101.

(25) Ataka, K.; Giess, F.; Knoll, W.; Naumann, R.; Haber-Pohlmeier, S.; Richter, B.; Heberle, J. Oriented Attachment and Membrane Reconstitution of His- Tagged Cytochrome c Oxidase to a Gold Electrode: In Situ Monitoring by Surface-Enhanced Infrared Absorption Spectroscopy. *J. Am. Chem. Soc.* **2004**, *126*, 16199–16206.

(26) Forbrig, E.; Staffa, J. K.; Salewski, J.; Mroginski, M. A.; Hildebrandt, P.; Kozuch, J. Monitoring the Orientational Changes of Alamethicin during Incorporation into Bilayer Lipid Membranes. *Langmuir* **2018**, *34*, 2373–2385.

(27) Gutiérrez-Sanz, O.; Forbrig, E.; Batista, A. P.; Pereira, M. M.; Salewski, J.; Mroginski, M. A.; Götz, R.; De Lacey, A. L.; Kozuch, J.; Zebger, I. Catalytic Activity and Proton Translocation of Reconstituted Respiratory Complex I Monitored by Surface-Enhanced Infrared Absorption Spectroscopy. *Langmuir* **2018**, *34*, 5703–5711.

(28) Wiebalck, S.; Kozuch, J.; Forbrig, E.; Tzschucke, C. C.; Jeuken, L. J. C.; Hildebrandt, P. Monitoring the Transmembrane Proton Gradient Generated by Cytochrome bo3 in Tethered Bilayer Lipid Membranes Using SEIRA Spectroscopy. *J. Phys. Chem. B* **2016**, *120*, 2249–2256.

(29) Terasaka, E.; Yamada, K.; Wang, P.-H.; Hosokawa, K.; Yamagiwa, R.; Matsumoto, K.; Ishii, S.; Mori, T.; Yagi, K.; Sawai, H.; Arai, H.; Sugimoto, H.; Sugita, Y.; Shiro, Y.; Tosha, T. Dynamics of Nitric Oxide Controlled by Protein Complex in Bacterial System. *Proc. Natl. Acad. Sci. U. S. A.* **2017**, *114*, 9888–9893.

(30) Yaguchi, M.; Uchida, T.; Motobayashi, K.; Osawa, M. Speciation of Adsorbed Phosphate at Gold Electrodes: A Combined Surface-Enhanced Infrared Absorption Spectroscopy and DFT Study. *J. Phys. Chem. Lett.* **2016**, *7*, 3097–3102.

(31) Miyake, H.; Ye, S.; Osawa, M. Electroless Deposition of Gold Thin Films on Silicon for Surface-Enhanced Infrared Spectroelectrochemistry. *Electrochem. Commun.* **2002**, *4*, 973–977.

(32) Kato, M.; Cardona, T.; Rutherford, A. W.; Reisner, E. Covalent Immobilization of Oriented Photosystem II on a Nanostructured Electrode for Solar Water Oxidation. *J. Am. Chem. Soc.* **2013**, *135*, 10610–10613.

(33) Barth, A. Infrared Spectroscopy of Proteins. *BBA Bioenergetics* **2007**, *1767*, 1073–1101.

(34) Mukherjee, S.; Chowdhury, P.; Gai, F. Infrared Study of the Effect of Hydration on the Amide I Band and Aggregation Properties of Helical Peptides. *J. Phys. Chem. B* **2007**, *111*, 4596–4602.

(35) Jiang, X.; Zaitseva, E.; Schmidt, M.; Siebert, F.; Engelhard, M.; Schlesinger, R.; Ataka, K.; Vogel, R.; Heberle, J. Resolving Voltage-Dependent Structural Changes of a Membrane Photoreceptor by Surface-Enhanced IR Difference Spectroscopy. *Proc. Natl. Acad. Sci. U. S. A.* **2008**, *105*, 12113–12117.

(36) Osawa, M.; Ikeda, M. Surface-Enhanced Infrared Absorption of P-Nitrobenzoic Acid Deposited on Silver Island Films: Contributions of Electromagnetic and Chemical Mechanisms. *J. Phys. Chem.* **1991**, *95*, 9914–9919.

(37) Osawa, M.; Ataka, K.-I.; Yoshii, K.; Nishikawa, Y. Surface-Enhanced Infrared Spectroscopy: The Origin of the Absorption Enhancement and Band Selection Rule in the Infrared Spectra of Molecules Adsorbed on Fine Metal Particles. *Appl. Spectrosc.* **1993**, *47*, 1497–1502.

(38) Heering, H. A.; Wiertz, F. G. M.; Dekker, C.; Vries, S. De. Direct Immobilization of Native Yeast Iso-1 Cytochrome c on Bare Gold : Fast Electron Relay to Redox Enzymes and Zeptomole Protein-Film Voltammetry. *J. Am. Chem. Soc.* **2004**, *126*, 6270–6276.

(39) Rüdiger, O.; Abad, J. M.; Hatchikian, E. C.; Fernandez, V. M.; De Lacey, A. L. Oriented Immobilization of Desulfovibrio Gigas Hydrogenase onto Carbon Electrodes by Covalent Bonds for Nonmediated Oxidation of H_2. *J. Am. Chem. Soc.* **2005**, *127*, 16008–16009.

(40) Spiro, T. G.; Wasbotten, I. H. CO as a Vibrational Probe of Heme Protein Active Sites. *J. Inorg. Biochem.* **2005**, *99*, 34–44.

(41) Lu, S.; Suharti; Vries, S. de; Moënne-Loccoz, P. Two CO Molecules Can Bind Concomitantly at the Diiron Site of NO Reductase from Bacillus Azotoformans. *J. Am. Chem. Soc.* **2004**, *126*, 15332–15333.

(42) Sato, N.; Ishii, S.; Sugimoto, H.; Hino, T.; Fukumori, Y.; Sako, Y.; Shiro, Y.; Tosha, T. Structures of Reduced and Ligand-Bound Nitric Oxide Reductase Provide Insights into Functional Differences in Respiratory Enzymes. *Proteins* **2014**, *82*, 1258–1271.

(43) Blomberg, M. R. A.; Siegbahn, P. E. M. Mechanism for N_2O Generation in Bacterial Nitric Oxide Reductase: A Quantum Chemical Study. *Biochemistry* **2012**, *51*, 5173–5186.

(44) Blomberg, M. R. A. Can Reduction of NO to N_2O in Cytochrome c Dependent Nitric Oxide Reductase Proceed through a Trans-Mechanism? *Biochemistry* **2017**, *56*, 120–131.

(45) Blomberg, L. M.; Blomberg, M. R. A.; Siegbahn, P. E. M. Reduction of Nitric Oxide in Bacterial Nitric Oxide Reductase—a Theoretical Model Study. *BBA Bioenergetics* **2006**, *1757*, 240–252.

(46) Abucayon, E. G.; Khade, R. L.; Powell, D. R.; Zhang, Y.; Richter-Addo, G. B. Lewis Acid Activation of the Ferrous Heme–NO Fragment toward the N–N Coupling Reaction with NO To Generate N_2O. *J. Am. Chem. Soc.* **2018**, *140*, 4204–4207.